

## **GAS Journal of Engineering and Technology (GASJET)**

Volume 2 | Issue 10, 2025

Homepage: <a href="https://gaspublishers.com/gasjet-home/">https://gaspublishers.com/gasjet-home/</a>



ISSN: 3048-5800

# Multi-Fault Diagnosis of Rotational Machinery based on AIS and BSS

Sung-Ri Kim, Kwang-Myong Ko, Hyon-Chol Choe

Faculty of Mechanical Science and Technology, Kim Chaek University of Technology, 60-Kyogu, Yonggwang Street, Pyongyang 950003, Democratic People's Republic of Korea

Received: 30.08.2025 | Accepted: 03.10.2025 | Published: 23.10.2025

\*Corresponding Author: Sung-Ri Kim

**DOI:** 10.5281/zenodo.17422240

Abstract Original Research Article

The multi-fault diagnosis of rotational machinery is one of the most difficult problems in machine fault diagnosis. When various kinds of faults co-exist, different fault symptoms are combined each other, therefore it is usually difficult to construct the mathematical model for faults and to perform reliable diagnosis. This paper proposes a multi-fault diagnosis method for rotating machinery coupling the advantages of artificial immune system (AIS), blind source separation (BSS) and data fusion theory. First, the mixed vibration signals measured by several sensors are separated into some single fault signals and noise by blind source separation. A major drawback of conventional BSS is that the contributions of acquired separation signals for source signals are undeterminant, i.e., the sum of separated signals is different from the source signal. This paper suggests an enhanced blind source separation matching source contributions of separated signals and finds new separation signals matching source contributions of separated signals. In addition, the immune detectors for diagnosing single fault diagnosis are constructed using AIS and the standard single fault samples presented by previous researchers. In order to improve the convergence of AIS and increase the variety of solution, a new objective function combining affinity information and density information is proposed. All separated signals are passed through immune fault detectors and the possibilities of the fault generation are found. Finally, the contributions of the separated signals for the source signals are found, and multi-fault is diagnosed by these contributions and data fusion theory. The comparison of presented and conventional method is performed. The effectiveness of the diagnosis method presented in this paper is verified by simulation and experiment.

Keywords: Multi-fault; Fault diagnosis; Rotating machinery; Artificial immune system; Blind source separation; Data fusion.

Copyright © 2025 The Author(s). This is an open-access article distributed under the terms of the Creative Commons Attribution-NonCommercial 4.0 International License (CC BY-NC 4.0).

#### 1. Introduction

A great deal successes have been achieved in the field of machinery fault diagnosis and widely used in the real process recently.

However, due to the complexity of machinery structures and works, there are a lot of difficulties in machinery fault diagnosis. Especially, when different kinds of faults co-exist, different fault features are combined each other, this makes it difficult to construct the mathematical model of faults and to perform reliable diagnosis.

Two main steps are required for fault diagnosis: feature extraction and classification of fault.

In order to extract fault features, measured vibrational signals should be processed by some signal processing methods, such as fast Fourier transform(FFT)[15], wavelet transform(WT)[16,17,21,26], empirical mode decomposition(EMD)[7,11] and blind source separation(BSS)[1-10], etc.

The multi-fault of rotating machinery can be classified using fault features obtained from separated signals and some machine learning tools.

There are different machine learning tools for classifying the multi-fault of rotating machinery, such as artificial neural network(ANN)[19], genetic



algorithm(GA)[23,24], support vector machines (SVM)[ 12,14,18], fuzzy identification(FI)[20], artificial immune system(AIS)[13,18], D-S theory of evidence[13] and principal component analysis(PCA)[22,25,26], etc.

Among different methods, empirical mode decomposition (EMD) is of particular interest because of its highly adaptive nature in analyzing vibrations. EMD decomposes a signal into a series of intrinsic mode functions(IMFs) according to the signal characteristics, allowing the non-stationary and nonlinearity information of the signal to be revealed for more accurate characterization of signals, for example, gear fault diagnosis and rolling bearing fault diagnosis[7,11]. However, EMD often cannot extract fault features accurately because of the problem of mode mixing [11].

The dual-tree complex wavelet transform [17] is one of the few techniques to extract the multiple fault signatures in the rotating machine.

If multiple sensors are used in the monitoring system, blind source separation (BSS) could be used to recover the unknown independent sources from observed signals mixed by an unknown propagation medium [6]. A drawback of traditional BSS is that the contributions of acquired separation signals for source signal are undeterminancy, i.e., the sum of separated signals is different from the source signal [9].

For a decade or so, the support vector machine (SVM) has been used widely in condition monitoring and fault diagnosis of machinery for the binary-fault classification of machine elements.

D.J. Bordoloi [12] indicated that among numerous methods available in faults classifications the application of SVM is still uncommon. Looking into tremendous information contained in wavelets an attempt in conjunction with the SVM and the optimization of SVM parameters for the multi-fault classification would be a worth effort, which is lacking in available literatures [17].

It is highly desirable to develop a fault diagnosis that can model and analyze diagnosis problems using uncertain information, which is likely to be incomplete and vague.

Due to the power of the D-S theory in handling uncertainties, so far, it has found many application areas, for example, expert system, uncertainty reasoning. To avoid the drawbacks of using evidential theory alone to fault diagnosis, for example, its heavy calculation burden due to the exponential "explosion" of the focal elements involved by fault information and data combination, Qing Hua Zhang and Qin Hu [13] presented an integrated approach for the concurrent fault diagnosis using artificial immune algorithm and evidential theory, aiming to not only improve the diagnostic rate but also increase the reliability of diagnostic conclusion.

This paper suggests a multi-fault diagnosis method using the single fault samples of rotating machinery.

To separate multi-fault signals, an enhanced blind source separation matching source contributions of separated signals and finds the contributions of the separated signals for the source signals.

In addition, the immune detectors for diagnosing single faults are constructed using AIS and the standard single fault samples presented by previous researchers. To improve the convergence of AIS and to increase the variety of solution, a new objective function combining affinity information and density information is proposed. All separated signals are passed through immune fault detectors and the possibilities of the fault generation are found.

Finally, the quantitative contributions of the separated signals for source signal are found, and multi-fault is diagnosed by these contributions and data fusion theory.

The comparison of presented and conventional method are performed. The effectiveness of the diagnosis method presented in this paper is verified by simulation and experiment.



#### 2. Theoretical background

### 2.1 Enhanced blind source separation

The main idea of blind source separation is to determine the most proper estimates y, finding separation matrix W under the condition in which independent source signal S and mixing matrix A are unknown. i.e.

$$y = W^T x = W^T A S \tag{1}$$

Where W is separation matrix.

Now there are several methods for determining separation matrix W.

The main idea of Minimal Mutual information (MMI) is to choose the weight matrix W of neural network, minimizing the interdependencies between output signals.

The expression [3] for correcting the weight matrix satisfying the condition to minimize the mutual information of separation signals is written as

$$\frac{dW}{dt} = \eta (I - \phi(y)y^{T})W \tag{2}$$

Where  $\eta$  is learning rate,  $\phi(\cdot)$  is series of nonlinear functions.

Using expression (2), final separation signal y is obtained.

This is the first stage for separating mixed vibration signal.

The obtained separation signals satisfy the condition minimizing mutual information, but the source contributions are unknown.

It is important to find source contributions quantitatively, especially for condition monitoring and fault diagnosis.

This paper proposes an enhanced blind source separation for finding the source contributions of separated signals quantitatively.

The main idea of the enhanced blind source separation is described as follows.

First, fast Fourier transform is performed for mixed signal x and separation signal y, and amplitude spectrum X and Y are found.

$$X(f) = \int_{-\infty}^{+\infty} x(t) \cdot e^{-j2\pi f t} dt$$
 (3)

$$Y(f) = \int_{-\infty}^{+\infty} y(t) \cdot e^{-j2\pi f t} dt$$
 (4)

The scaled signals are written as

$$\overline{Y} = \alpha Y \tag{5}$$

Where  $\alpha$  is scaling coefficient matrix of separated signals, Y is separation signal vector, and  $\overline{Y}$  is scaled separation signal vector.

Then the sum of scaled separation signals should be similar to the mixed source signal measured from sensor, therefore following objective function will be satisfied:

$$F(\alpha) = \sum_{i=1}^{N/2} (X_{ij} - \sum_{k=1}^{n_s} \overline{Y}_{kj})^2, \quad i = 1, 2, \dots, n_s : \min$$
 (6)

Substituting Expression (5) into expression (6) yields

$$F(\alpha) = \sum_{i=1}^{N/2} (X_{ij} - \sum_{k=1}^{n_s} \alpha_{ik} Y_{kj})^2, \quad i = 1, 2, \dots, n_s : \min$$
 (7)

Where N is the sampling length of measured signal and  $n_s$  is the number of source signals.

From the extremal condition of expression (7), following  $n_s \times n_s$  linear equations are obtained:

$$G(\boldsymbol{\alpha}) = \sum_{j=1}^{N/2} Y_{mj} X_{ij} - \sum_{j=1}^{N/2} \sum_{k=1}^{n_s} \alpha_{ik} Y_{kj} Y_{mj} = 0, \quad i = 1, 2, \dots, n_s, \quad m = 1, 2, \dots, n_s \quad (8)$$

Solving equation (8), scaling coefficient matrix  $\alpha$  is obtained.

From expression (5), scaled approximate separation signals are obtained.

These signals not only don't change mutual information, but also satisfy real scales for source signals.

This process will be performed every stage.

Performing Fourier inverse transform for modified signals, scaled time domain signal  $\bar{y}(t)$  is obtained.

$$\overline{y}(t) = \int_{-\infty}^{+\infty} \overline{Y}(f) \cdot e^{j2\pi t f} df \tag{9}$$

Then expression (2) can be modified as

$$\frac{dW}{dt} = \eta (I - \phi(\bar{y})\bar{y}^T)W \tag{10}$$

The expression (10) is a formula for correcting weight matrix of the enhanced **BSS**.

This is the second stage for finding source contributions of separated signals.

#### 2.2. Algorithm for generating AIS fault detectors

#### 2.2.1. Main steps of AIS learning algorithm

Artificial Immune system (AIS) has many abilities such as learning, memory, self-regulation, and pattern recognition and feature extraction and so on [18].

This paper uses Clone Selection Algorithm (CSA) of AIS to create immune fault detectors.

AIS learning algorithm consists of following steps:

i) The *i*th fault sample to be trained is  $Ag_i$ , antigen (a set of fault sample) is written as  $Ag = (Ag_1, Ag_2, \dots, Ag_b)$ .

The size of population N, maximum clone size  $N_c$ , convergence error  $\varepsilon$  and generation T are selected and memory matrix M is initialized.

ii) A set of antigen is inputted to the network and n

antibody  $Ab_n$  are generated randomly.

- iii) If stopping condition isn't satisfied, following loop is performed:
- (i) Following steps are performed for every antigen  $Ag_i$  of antigen Ag.
- ①The affinities between every antibody  $Ab_{\{N\}}$  and antigen  $Ag_i$  are calculated.
- (2) The density of antibody  $Ab_{\{N\}}$  is calculated.
- ③The antibodies, whose density affinities are larger than threshold  $t_p$  are selected and they are selected as the clone antibody collection of next generation.
- (4) Creating the clone cells for the selected antibody collection, clone antibody populations  $Ab_j$  are constructed.



 $\bigcirc$  Performing mutation for clone antibody populations  $Ab_j$ , clone mutation antibody populations  $Ab_i^*$  are constructed.

**6** Calculating affinities between clone mutation antibody population  $Ab_j^*$  and antigen  $Ag_i$ , selecting  $\beta$  antibodies, whose affinities are large relatively, and new antibody population  $Ab_j^{**}$  is constructed.

⑦Calculating the similarity coefficients between antibodies in antibody populations  $Ab_j^{**}$ , suppressing antibodies, whose thresholds larger than threshold  $t_s$ , memory cell population  $m_i$  is obtained for antigen  $Ag_i$ .

(ii) Suppressing antibodies whose densities  $D_i$  are larger than threshold  $t_a$  in total memory matrix M, memory cell population  $M_e$  is obtained for every antigen.

Creating antibodies randomly and adding them to memory cell population, new antibody population is constructed and we return to step (1)

iv) Iteration is halted.

Halting condition of algorithm is to reach a fixed order T.

After completing iteration, we can obtain finally the memory cell population  $M_e$  for every antigen.

## 2.2.2. Calculation of AIS parameters

Using following expressions, the parameters of AIS are calculated:

(1) Affinity

The normalized Euclidean distance between antigen  $Ag_i$  and antibody  $Ab_j$  is represented as:

$$d_{ij} = \frac{\sqrt{\sum_{k=1}^{m} (Ag_{ik} - Ab_{jk})^2}}{\sum_{k=1}^{m} Ag_{ik}}$$
(11)

Then, affinity can be calculated as:

$$F_{ij} = \frac{1}{1 + \beta d_{ii}} \tag{12}$$

In order to limit the range of  $F_{ij}$  to 0~1, we choose  $1\times10^4$  for  $\beta$ .

It's shown that affinity increases if the distance between antigen and antibody decreases.

2)Stimulation degree and density of antibody

The antibodies whose densities are close each other in some degree are regarded as identical antibodies.

From the physical meaning of antibody, its density can be written as

$$D_{i} = \frac{\sum_{j=1}^{n} W_{ij}}{n}$$

$$W_{ij} = \begin{cases} 1 & S_{ij} \ge t_{a} \\ 0 & S_{ij} < t_{a} \end{cases}$$
(13)

Where  $D_i$  is the density of *i*th antibody,  $W_{ij}$  is the stimulation degree of antibody,  $S_{ij}$  is the similarity between antibody *i* and *j*, ta is density threshold, and *n* is total number of antibody.

The similarity between antibodies i and j can be represented as:

$$S_{ij} = \frac{1}{1 + \lambda H_{ij}}$$

$$H_{ij} = \frac{\sqrt{\sum_{k=1}^{m} (Ab_{ik} - Ab_{jk})^2}}{\sum_{k=1}^{m} Ab_{ik}}$$
(14)

Where  $H_{ii}$  is the distance function between antibody i and j, we select  $\lambda$  as  $1\times10^4$ , similarly to expression (12).

Expression (13) shows that the more there are similar antibodies in the memory cell, the more stimulation degree and density increase, and Expression (14) shows that the smaller the distance between an antibody and another antibody is, the more the similarity between them increases.

In order to increase the affinity, to decrease the density and to improve the variety of antibodies, This paper proposes following objective function:

$$J_{ij} = \eta_1 F_{ij} + \frac{\eta_2 \theta}{\xi D_i + \theta} : \max$$
 (15)

Where  $\theta = 1 \times 10^{-3}$  and  $\xi = 1 \times 10^{4}$ .

From expression (15), if 
$$D_i = 0$$
,  $\frac{\theta}{\xi D_i + \theta} = 1$ , and, if  $D_i = 1$ ,  $\frac{\theta}{\xi D_i + \theta} \approx 0$ .

Also,  $\eta_i$  is the weight coefficient for density and affinity, we can select it to satisfy  $\sum \eta_i = 1$ .

In this paper, we select 0.65 and 0.35 for  $\eta_1$  and  $\eta_2$ , respectively.

It's shown that the larger the affinity between antigen and antibody is and the smaller the density of antibody is, the more the objective function increases.

Using expression (15), in the initial stage, we can choose the antibodies whose affinities are larger and similarities are smaller, so we can increase the convergence speed of the algorithm and improve the variety of antibodies. The framework of the algorithm is shown in Figure 1.

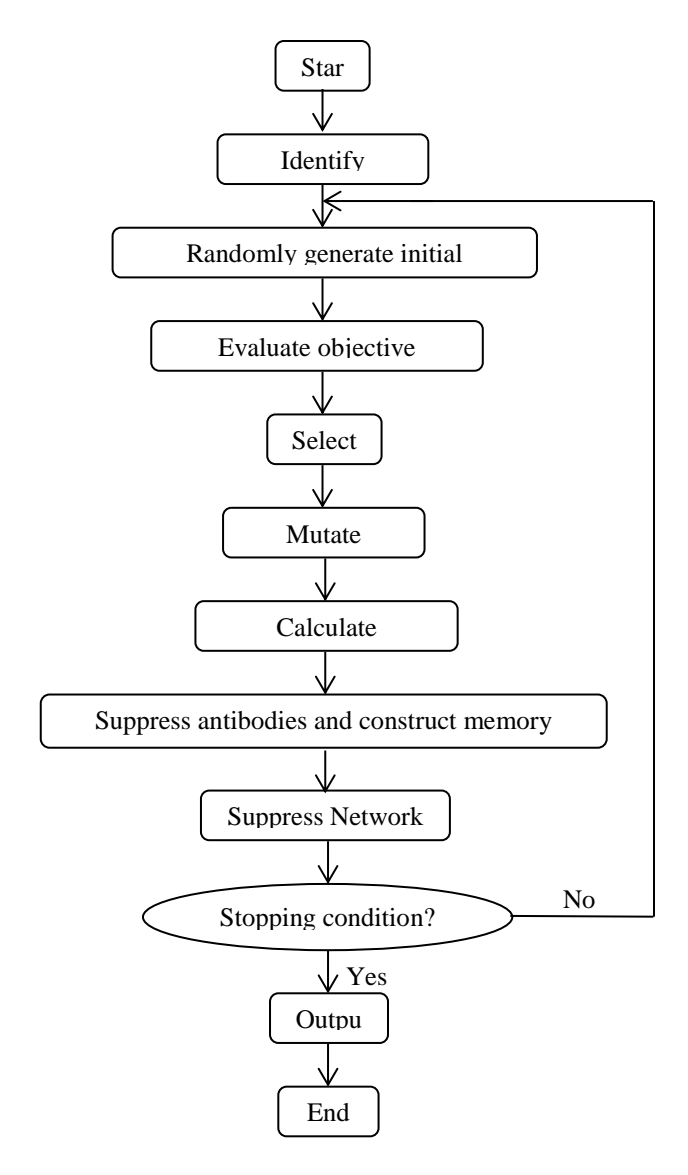


Fig1. Fault detector generation algorithm based on CSA

## 3. Multi-fault diagnosis of rotating machinery

#### 3.1 Simulation of enhanced BSS algorithm

In order to verify the effectiveness of proposed enhanced **BSS** algorithm, by mixing following signals, simulation for separating signals is performed:

$$s_1 = 0.75\cos(2\pi f_1 t)$$

$$s_2 = 0.25 sign \left[\cos(2\pi f_2 t)\right]$$

$$s_3 = randn(t)$$

The time waves of source signals are shown as figure 2, 3 and 4.



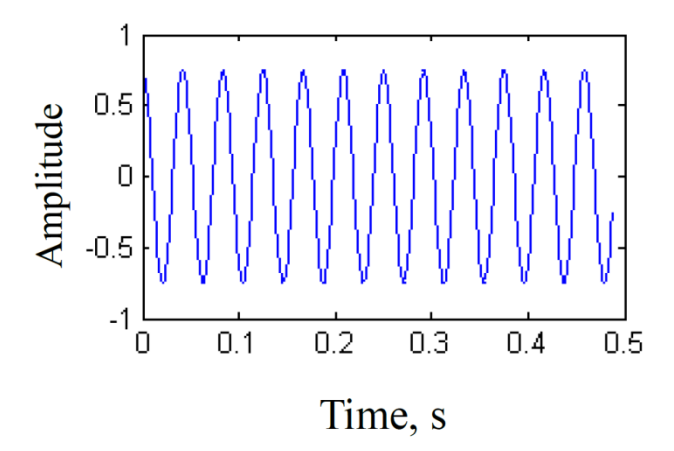


Fig 2.Time waves of source signal 1

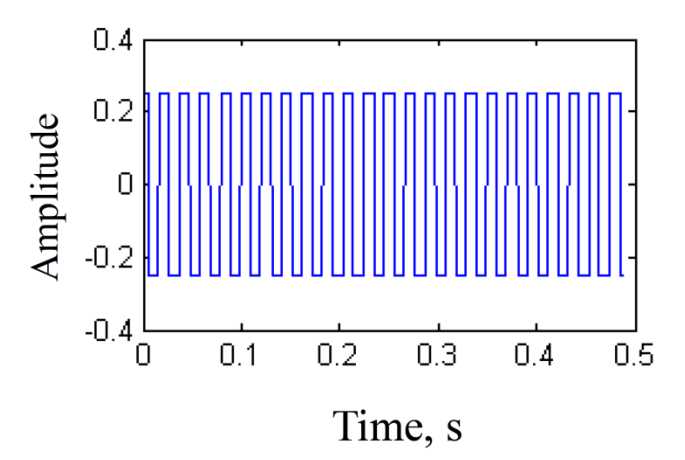


Fig 3.Time waves of source signal 2

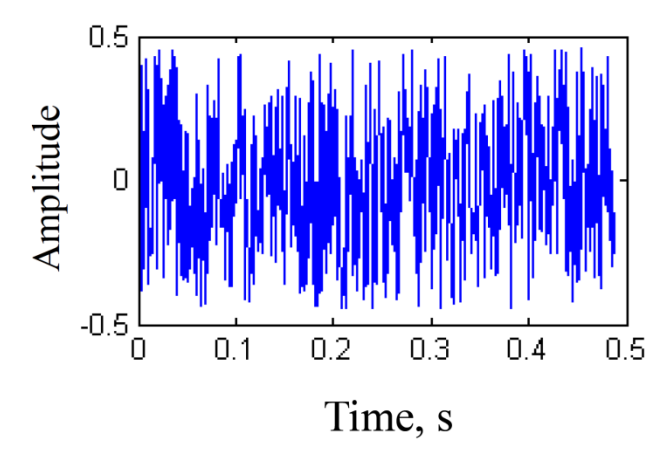


Fig 4.Time waves of source signal 3



The mixing matrix is given by following matrix of random number:

$$A = \begin{bmatrix} 0.1245 & 0.2856 & 0.6834 \\ 0.2143 & 0.1362 & 0.5365 \\ 0.3456 & 0.2356 & 0.6435 \end{bmatrix}$$

Following mixed signals are obtained using the source signals and the mixing matrix:

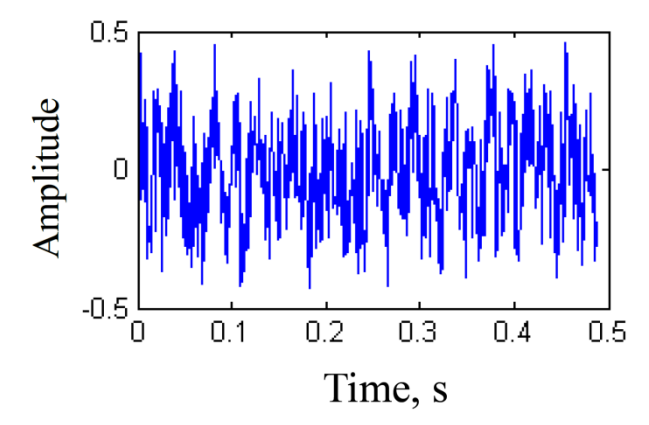


Fig5.Time waves of mixed signal 1

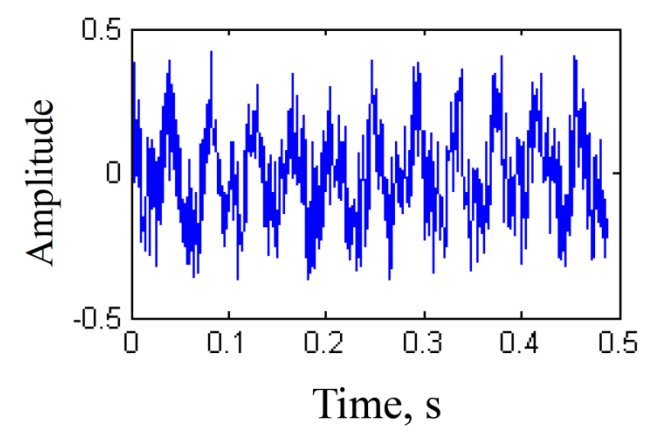


Fig6. Time waves of mixed signal 2

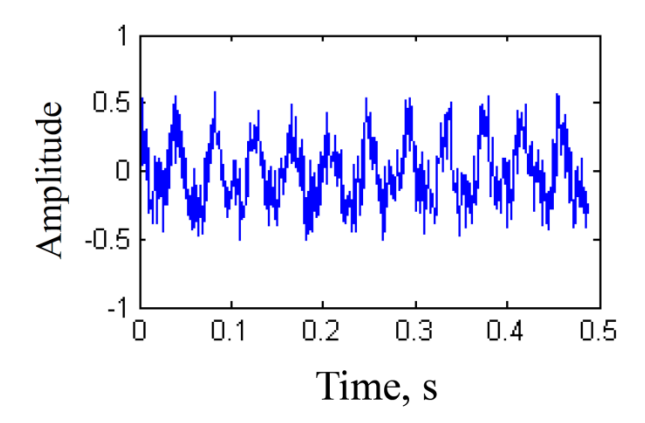


Fig7.Time waves of mixed signal 3

The algorithm was converged after about 5000 iterations (Figure 8, 9 and 10).

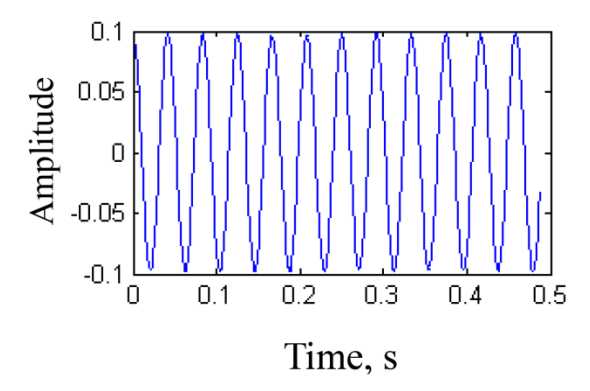


Fig 8. Time wave of separation signal 1

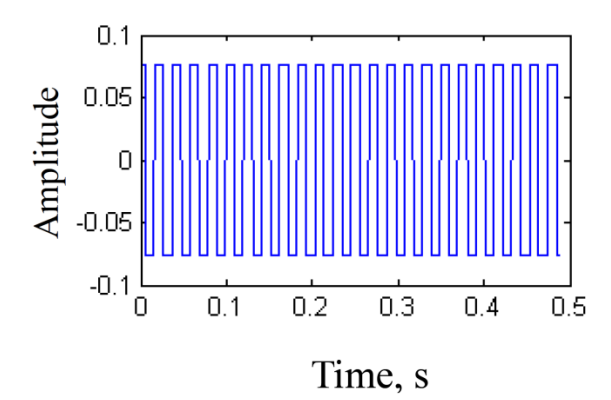


Fig 9. Time wave of separation signal 2



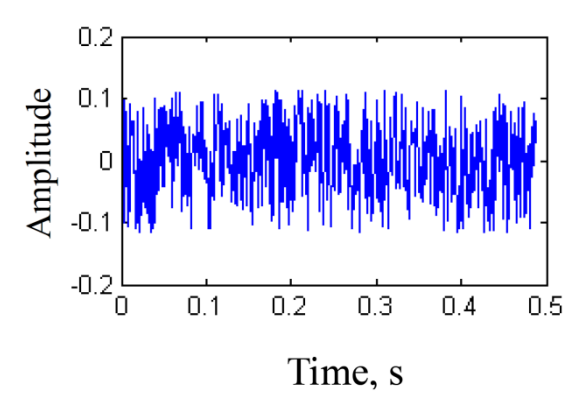


Fig 10. Time wave of separation signal 3

Figure 8, 9 and 10 show that the separated signals are different from the source mixed signals in their scales.

Then, separation simulation is performed using the proposed enhanced **BSS** algorithm.

The obtaibed scaling coefficient matrix is:

$$\alpha = \begin{bmatrix} 0.948 & 1.643 & 2.650 \\ 2.668 & 2.096 & 2.508 \\ 0.9042 & 0.422 & 0.743 \end{bmatrix}$$

Figure 11 and 12 show the source mixed signal and the composed signal.

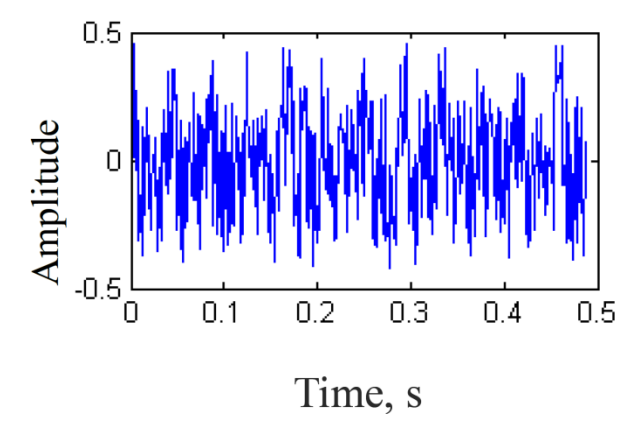


Fig 11. Mixed signal



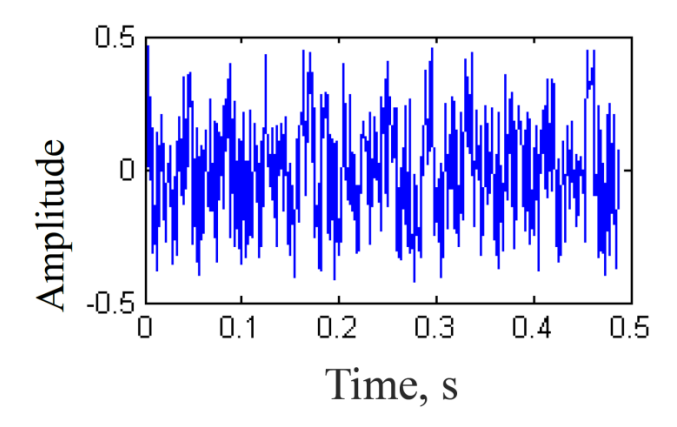


Fig 12. Composed signal

Figure 11 and 12 show that the source signals are almost identical with the composed signals...

It's shown that the enhanced **BSS** algorithm proposed in this paper doesn't change the mutual information of signals and also can maintain the source contributions of separated signals.

3.2 Generation of single fault detectors

The power spectrum components are obtained for 7 typical faults and 9 frequency bands.

The peak values are found for every frequency band and defined by  $E_i$ ,  $i = \overline{1, n}$ .

In order to use it as the input data of CSA,  $E_i$  are normalized as following dimensionless parameters:

$$X_{i} = E_{i} / \sum_{k=1}^{n} E_{k} \quad i = \overline{1, n}$$
 (16)

$$X_i$$
 are in range of 0~1 and satisfy  $\sum_{i=1}^n X_i = 1$ .

Following vector are constructed by the calculated parameters:

$$\mathbf{A} = [X_1, X_2, X_3, X_4, X_5, X_6, X_7, X_8, X_9] \tag{17}$$

Expression (17) is used for the training sample to generate single fault detectors.

Table 1 shows the training samples for 7 typical rotor faults.

Table 1. Detector training samples for 7 typical rotor faults

N o	Fault pattern	Spectrum energy distribution									
		Frequency band									
		0.01	0.4	0.5 <i>f</i>	0.51 ~0.9	1 <i>f</i>	2 f	3~	Odd times	\5 f	
		0.39	0.49	$0.5f_{\rm n}$	$9 f_{\rm n}$	$1 f_{\rm n}$	$2f_{\rm n}$	$5f_{\rm n}$	of $f_n$	$>5 f_{\rm n}$	

		$f_{\rm n}*$	$f_{n}$							
1	Unbalance	0.0	0.0	0.0	0.0	0.9	0.0 5	0.0 5	0.0	0.0
2	Rotor radial friction	0.1	0.1	0.0	0.1	0.2	0.1	0.2	0.1	0.1
3	Misalignment	0.0	0.0	0.0	0.0	0.4	0.5	0.1	0.0	0.0
4	Rotor cracking	0.0	0.0	0.0	0.4	0.2	0.2	0.0	0.0	0.2
5	Bearing looseness	0.5	0.4	0.0	0.0	0.0	0.0	0.1	0.0	0.0
6	Casing support looseness	0.3	0.2	0.0	0.0	0.0	0.0	0.0	0.5	0.0
7	Oil film resonance	0.0	1.0	0.0	0.0	0.0	0.0	0.0	0.0	0.0

\*  $f_n$  is the frequency of rotation.

100 fault detectors are generated for every fault.

Figure 13~22 show 5 fault detectors for every fault.

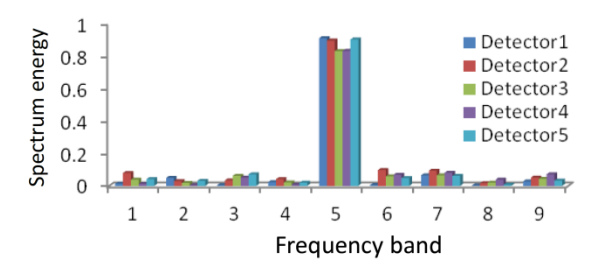


Fig13. Immune Fault Detectors of unbalance

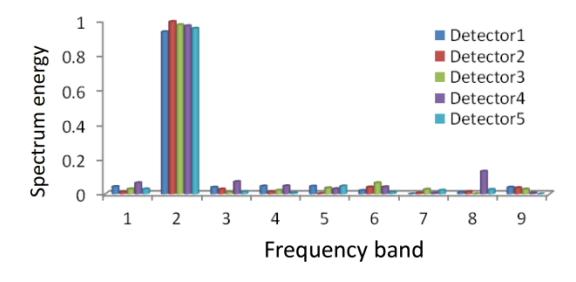


Fig14. Immune Fault Detectors of oil film resonance

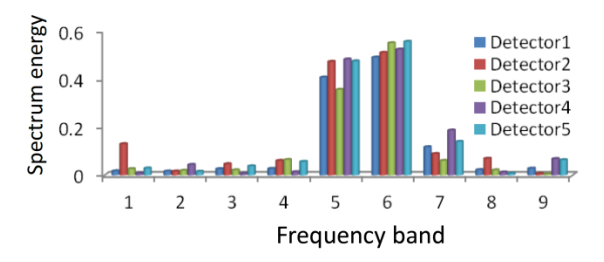




Fig15. Immune Fault Detectors of misalignment

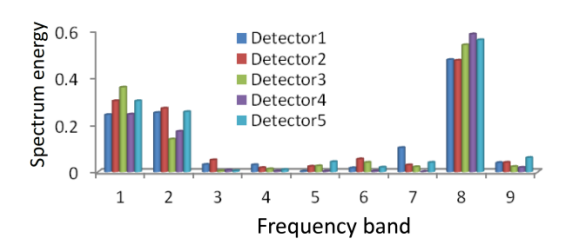


Fig16. Immune Fault Detectors of misalignment

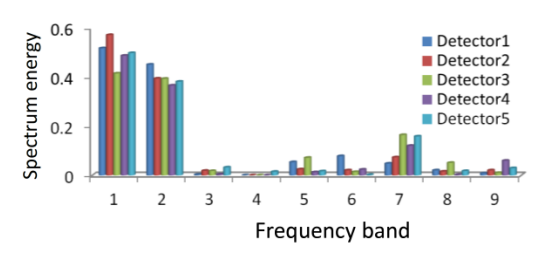


Fig 17. Immune Fault Detectors of casing support looseness

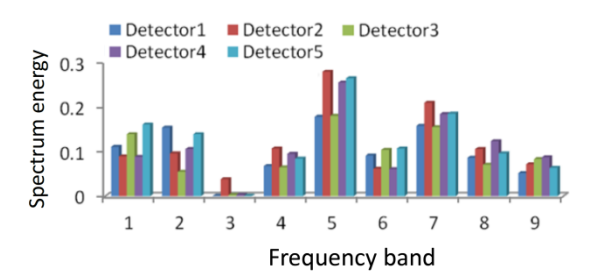


Fig 18. Immune Fault Detectors of rotor radial friction

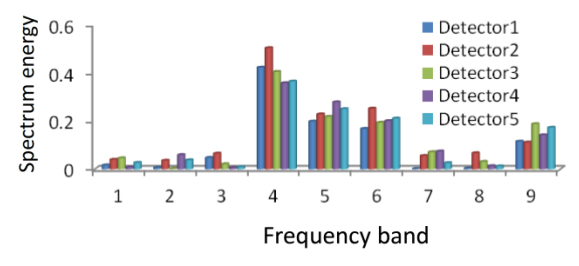


Fig 19. Immune Fault Detectors of rotor cracking

The contributions of separated signals for source signals are defined as



$$c_{mn} = \frac{\sum_{j=1}^{N/2} \overline{Y}_{nj}^{2}}{\sum_{j=1}^{N/2} X_{mj}^{2}}$$
(18)

Where 
$$m = \overline{1, n_s}$$
,  $n = \overline{1, n_s}$ 

The number of detectors for a fault type  $i(i=1,\dots,k,k)$  is the number of faults) is given as N.

Comparing the fault feature vector for separation signals with every fault detector, if the Euclidean distance between them is less than a threshold, 1 is added to the concerned counter  $D_{ij}$ .

The possibility of *j*th separation signal belonging to *i*th fault can be written as:

$$\eta_{ij} = D_{ij} / N, \quad i = \overline{1, n_s}, \quad j = \overline{1, n_s}$$
(19)

Determining fault generating possibilities for  $n_s$  separation signals and performing data fusion, the fault scores are calculated for every fault as:

$$S_{i} = \sum_{i=1}^{n_{s}} c_{ij} \cdot \eta_{ij}, \ i = \overline{1, n_{s}}$$
 (20)

Arranging these values in order, the types and intensity of fault can be evaluated quantitatively.

#### 4. Application example

#### 4.1 Test rig

In this research work, the test rig(Dynamics Key Laboratory, Kim Chaek University of Technology, DPRK) shown in Figure 20 is used to measure vibrational data, which consists of six parts such as motor, rotor, accelerometer, preamplifier, invertor and data acquisition.

Two sensors are mounted in horizontal and vertical directions of rotor to acquire fault signals from the test rig.

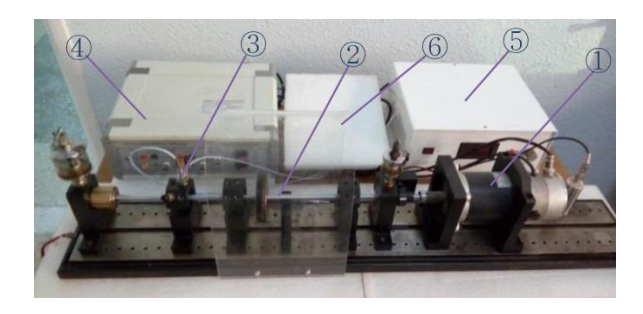


Fig 20. Test rig for rotor fault simulation: (1) motor, (2) rotor, (3) accelerometer, (4) preamplifier, (5) invertor, (6) data acquisition

Using the test rig, multi-faults of rotor such as unbalance combined with misalignment et al. can be simulated.

## 4.2 Multi-fault diagnosis

Unbalance and misalignment are simulated in

the test rig, and vibrational signals are measured by two piezoelectric acceleration sensors installed on the bearing housing horizontally and vertically.

The vibrational signals measured with 2 sensors and their spectrum diagrams are shown as Figure 21, 22, 23 and 24.

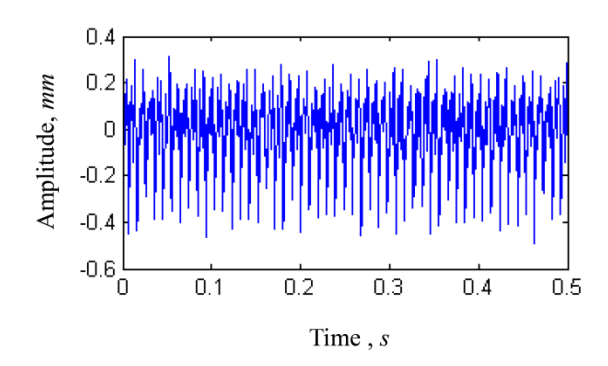


Fig 21. Time wave of vibration signal in sensor 1

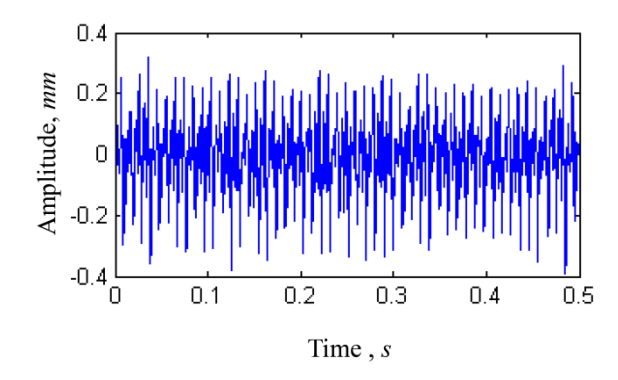


Fig 22. Time wave of vibration signal in sensor 2

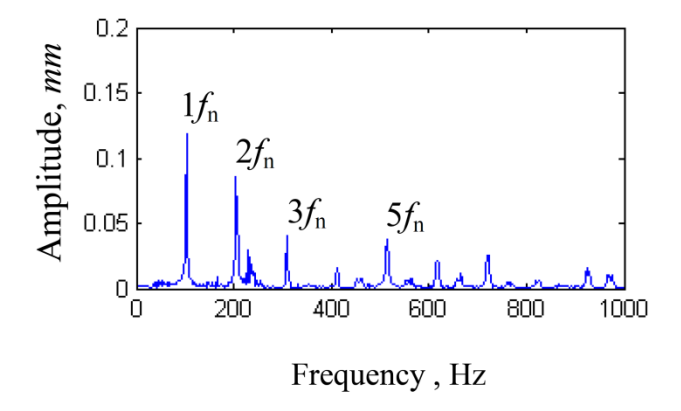


Fig 23. Spectrum Diagram of vibration signal for sensor 1

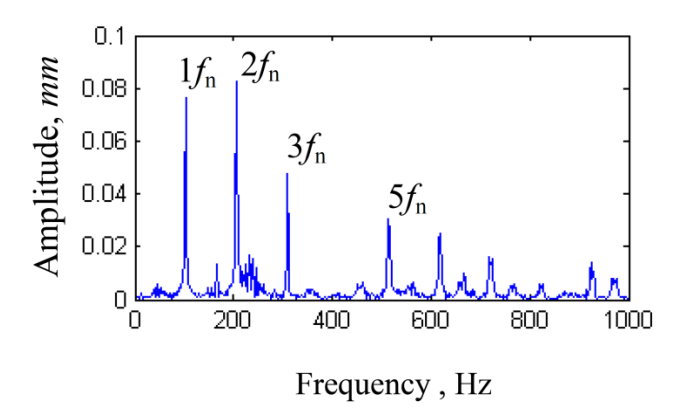


Fig 24. Spectrum Diagram of vibration signal for sensor 2

The frequency  $f_n(103.5\text{Hz})$  corresponds to the frequency for rotational speed(6 200r/min) of Figure 23 and 24.

For the vibration signals shown in Figure 23 and 24, signal separations are performed using the enhanced **BSS.** 

After 6 000 iterations, the algorithm is converged.

Figure 25, 26, 27, and 28 show the time waves and spectrum diagrams after separations.

As shown in Figure 28, the vibrational component corresponding to two times of rotational frequency, is eliminated in a large amount and unbalance fault feature is shown more obviously.

On the other hand, as shown in Figure 27, the vibrational component corresponding to two times of rotational frequency and the vibrational component corresponding to rotational frequency are shown concurrently.

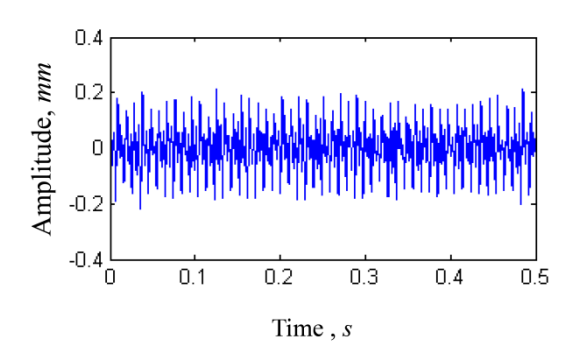


Fig 25. Time wave of vibration signal of channel 1

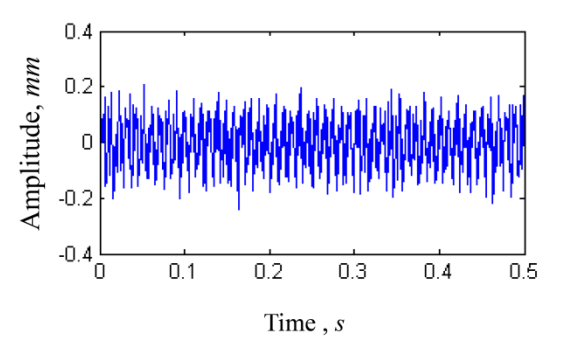


Fig 26. Time wave of vibration signal of channel 2

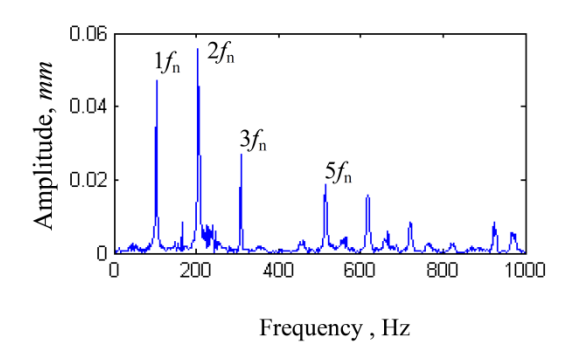


Fig 27. Spectrum Diagram of vibration signal of channel 1

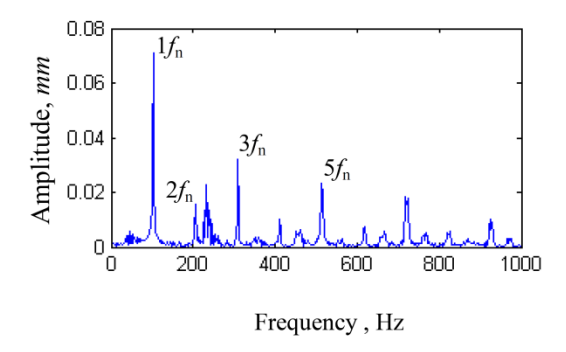


Fig 28. Spectrum Diagram of vibration signal of channel 2

The diagnosis result is shown in table 2.

The diagnosis result shows that separated signal 2 is caused by unbalance and separated signal 1 is caused by misalignment.

The fault diagnosis is performed for the separated signals using immune detectors.



	fault type										
No	unbalance	friction	misalignment	crack	bearing looseness	casing support looseness	oil film resonance				
Separation signal 1	0.920	0.000	0.080	0.000	0.000	0.000	0.000				
Separation signal 2	0.180	0.000	0.820	0.000	0.000	0.000	0.000				

Table 2. Fault diagnosis result

So, we can diagnose that the multi-fault by unbalance and misalignment is generated in the rotor From table 2, the score matrix for every fault is:

$$\eta = \begin{bmatrix} 0.920 & 0.080 \\ 0.180 & 0.820 \end{bmatrix} \tag{21}$$

The contributions of separation signals 1 and 2 are obtained as:

$$C = \begin{bmatrix} 0.461 & 0.472 \\ 0.583 & 0.527 \end{bmatrix} \tag{22}$$

Using table 2 and expression (21), the data fusion is performed as:

$$S = \begin{bmatrix} 0.920 \times 0.461 + 0.080 \times 0.472 \\ 0.180 \times 0.583 + 0.820 \times 0.527 \end{bmatrix} = \begin{bmatrix} 0.462 \\ 0.537 \end{bmatrix}$$
 (23)

From expression (23), we can evaluate quantitatively that the intensities of unbalance and misalignment are 46.2% and 53.7%, respectively.

#### Conclusion

This paper suggests an enhanced blind source separation and applies to find new separation signals matching source contributions of separated signals.

In addition, the immune detectors for diagnosing single faults are constructed using AIS and the standard single fault samples presented by previous researchers.

In order to improve the convergence of AIS and to increase the variety of solution, a new objective function combining affinity information and density information is proposed.

All separated signals are passed through immune

fault detectors and the possibilities of the fault generation are found.

Finally, the contributions of separated signals for the source signal are found, and multi-fault is diagnosed using these contributions and data fusion theory.

The effectiveness of the diagnosis method presented in this paper is verified using the simulation and the comparison to the traditional method and the experimental data.

### Acknowledgement

The major part of this study was supported by the Ministry of Education, the Guidance Bureau of Passenger Service in Pyongyang and Kim Chaek



University of Technology. The authors would like to thank the anonymous reviewers for their valuable and detailed comments and suggestions.

#### **REFERENCES**

- [1] Dong Wang, Peter W.Tse, A new blind fault component separation algorithm for a single-channel mechanical signal mixture, Journal of Sound and Vibration 331 (2012) 4956–4970.
- [2] J. Antoni, S.Chauhan, A study and extension of second-order blind source separation to operational modal analysis, Journal of Sound and Vibration 332 (2013) 1079–1106.
- [3] Linke Zhang, Yong Jiang, Bidirectional coupled noise sources separation over the same frequency band using convolutive blind separation method, Applied Acoustics 74 (2013) 301–306.
- [4] Lin He, Blind separation to improve classification of traffic noise, Applied Acoustics 72 (2011) 590–598.
- [5] Zhixiong Li, Xinping Yan, Blind vibration component separation and nonlinear feature extraction applied to the nonstationary vibration signals for the gearbox multi-fault diagnosis, Measurement 46 (2013) 259–271.
- [6] V.H. Nguyen, C. Rutten and J.-C. Golinval, Fault diagnosis in industrial systems based on blind source separation techniques using one single vibration sensor, Shock and Vibration 19 (2012) 795–801.
- [7] Jinjiang Wang1, Robert X. Gao1 and Ruqiang Yan, Integration of EEMD and ICA for wind turbine gearbox diagnosis, Wind Energy 17 (2014) 757–773.
- [8] N. Bouguerriou1, M. Haritopoulos2, C. Capdessus, L. Allam, Novel cyclostationarity-based blind source separation algorithm using second order statistical properties: Theory and application to the bearing defect diagnosis, Mechanical Systems and Signal Processing 19 (2005) 1260–1281.
- [9] N. Bouguerriou1, M. Haritopoulos2, C. Capdessus, L. Allam, Source Contribution Evaluation of Mechanical Vibration Signals via Enhanced Independent Component Analysis,

- Transactions of the ASME: Journal of Manufacturing Science and Engineering 4(134) (2012) 021014 1-9.
- [10] Xianhua Liu, Jean-Francois Cardoso, Robert B. Randall, Very fast blind source separation by signal to noise ratio based stopping threshold for the SHIBBS/SJAD algorithm, Mechanical Systems and Signal Processing 24 (2010) 2096–2103.
- [11] Zhijian Wang a, Zhennan Han a,n, Fengshou Gu a,b, et al. A novel procedure for diagnosing multiple faults in rotating machinery, ISA Transactions 55 (2015) 208–218
- [12] D.J. Bordoloi, Rajiv Tiwari, 2. Support vector machine based optimization of multi-fault classification of gears with evolutionary algorithms from time–frequency vibration data, Measurement 55 (2014) 1–14
- [13] Qing-Hua Zhang, Qin Hu, Guoxi Sun, Concurrent Fault Diagnosis for Rotating Machinery Based on Vibration Sensors, International Journal of Distributed Sensor Networks 472675 (2013) 10.
- [14] Zuqiang Su, Baoping Tang, Ziran Liu, et al. Multi-fault diagnosis for rotating machinery based on orthogonal supervised linear local tangent space alignment and least square support vector machine, Neurocomputing 157 (2015) 208–222
- [15] Identification of multiple transient faults based on the adaptive spectral kurtosis method, Journal of Sound and Vibration 331 (2012) 470–486
- [16] Jun Wang, Qingbo He, Fanrang Kong, An improved multiscale noise tuning of stochastic resonance for identifying multiple transient faults in rolling element bearings, Journal of Sound and Vibration 333 (2014) 7401–7421
- [17] Yanxue Wang, Zhengjia He, Yanyang Zi, Enhancement of signal denoising and multiple fault signatures detecting in rotating machinery using dual-tree complex wavelet transform, Mechanical Systems and Signal Processing 24 (2010) 119–137
- [18] Shengfa Yuan, Fulei Chu, Fault diagnosis based on support vector machines with parameter optimisation by artificial immunisation algorithm, Mechanical Systems and Signal Processing 21 (2007)



1318-1330

- [19] E. Cabal-Yepez, M. Valtierra-Rodriguez, R.J. Romero-Troncoso, et al. FPGA-based entropy neural processor for online detection of multiple combined faults on induction motors, Mechanical Systems and Signal Processing 30 (2012) 123–130
- [20] ZHANG Ming-jun, WU Juan, CHU Zhenzhong, Multi-Fault Diagnosis for Autonomous Underwater Vehicle Based on Fuzzy Weighted Support Vector Domain Description, China Ocean Eng 28(5) (2014) 599 616.
- [21] V. Purushothama, S. Narayanana, Suryanarayana A.N. Prasad, Multi-fault diagnosis of rolling bearing elements using wavelet analysis and hidden Markov model based fault recognition, NDT&E International 38 (2005) 654–664
- [22] Zhenyu Kong, Dariusz Ceglarek, Wenzhen Huang, Multiple Fault Diagnosis Method in Multistation Assembly Processes Using Orthogonal Diagonalization Analysis, Journal of Manufacturing Science and Engineering FEBRUARY 130 (011014)

(2008) 1-10

- [23] D.J. Bordoloi, Rajiv Tiwari, Optimum multifault classification of gears with integration of evolutionary and SVM algorithms, Mechanism and Machine Theory 73 (2014) 49–60
- [24] D.J. Bordoloi, Rajiv Tiwari, Support vector machine based optimization of multi-fault classification of gears with evolutionary algorithms from time–frequency vibration data, Measurement 55 (2014) 1–14
- [25] Renping Shao, Wentao Hu, Yayun Wang, The fault feature extraction and classification of gear using principal component analysis and kernel principal component analysis based on the wavelet packet transform, Measurement 54 (2014) 118–132
- [26] Zhixiong Li, Xinping Yan, Chengqing Yuan, Virtual prototype and experimental research on gear multi-fault diagnosis using wavelet-autoregressive model and principal component analysis method, Mechanical Systems and Signal Processing 25 (2011) 2589–2607